IEEJ Journal of Industry Applications
Vol.8 No.2 pp.152–159 DOI: 10.1541/ieejjia.8.152

Paper

Fast Force Control without Force Sensor Using Combination of aaKF and RFOB for In-circuit Test with Probing System

Sakahisa Nagai[*] Student Member, Roberto Oboe[**] Member
Tomoyuki Shimono[*,***] Senior Member, Atsuo Kawamura[*,***] Fellow

(Manuscript received March 12, 2018, revised Sep. 14, 2018)

The in-circuit test is performed by pushing a needle-type probe into the printed circuit board (PCB) and measuring the conductivity between the electronic components. To reduce the testing time and improve the test reliability, a swift and stable motion of the probe is required, especially when the probe touches the surface of the PCB. Instead of the conventional method involving the use of a force sensor, this study investigates the application of a micro electronical mechanical systems accelerometer to realize the quick contacting motion. The detection of the contact instant is evaluated by the jerk signal from this device. Subsequently, a negative force is added to the probe and the proposed force control based on acceleration aided Kalman filter and reaction force observer is applied. The experimental verification indicates that the settling time is reduced to approximately 10 ms and this corresponds to nearly 1% of the comparison data based on the existing technique.

Keywords: probing system, force control, acceleration aided Kalman filter, reaction force observer

1. Introduction

In-circuit tests are conducted for quality checking of printed circuit board (PCB) during their manufacturing process, to guarantee high reliability of the final products [(1)]. Probing systems with flying probes, in which a set of conductive needles is automatically positioned on test points of the device under test, are gaining importance in the in-circuit tests [(2)–(4)], thanks to their flexibility. In Ref. (2), a flying probe test circuit was designed to test the voltage of the probe resistance and pressure in real time. In Ref. (3), the minimum cost path of the probe was proposed to shorten the test time. Position control is usually applied in the probing systems and the test time can be reduced by moving the probes at high speed. However, contact oscillations are sometimes generated when the tip of a probe touches a test point of a PCB (printed circuit board) with high speed. The impact force and the oscillations may damage the soldering point and make the quality of the products worse. In Ref. (4), a probing system, which consists of a combination of a macro actuator and a micro actuator, makes use of a contact control strategy, aimed at reducing the impact force and the oscillation. However, the two actuators need to be controlled in a coordinated way and the system is complex.

[*] Division of Electrical and Computer Engineering, Yokohama National University
79-5, Tokiwadai, Hodogaya-ku, Yokohama, Kanagawa 240-8501, Japan
[**] Department of Management and Engineering, University of Padova, Stradella San Nicola
3, 36100 Vicenza, Italy
[***] Kanagawa Institute of Industrial Science and Technology
3-2-1, Sakado, Takatsu-ku, Kawasaki, Kanagawa 213-0012, Japan

Impact force control is also very important in other applications [(5)(6)]. In Ref. (5), a contact control for quick and smooth motion was proposed. The impact force and settling time were reduced by the braking motion and integral proportional force control. In Ref. (6), the impact force which is applied to a humanoid robot was suppressed by controlling the arm motion.

In all the systems mentioned above, a force sensor is used to detect and control the impact force. However, a large force sensor has disadvantages, such as some weakness against the impact force and it is also expensive. As a force sensorless system, reaction force observer (RFOB) has been proposed which can estimate the contact force without a force sensor [(7)].

A low pass filter (LPF) is applied to the RFOB output in order to reduce the measurement noise. Therefore, it is difficult for the RFOB to detect a very short time lasting impact force. In this study, a micro electronical mechanical systems (MEMS) accelerometer is used to detect the impact instant. Additionally, the accelerometer is used to improve the performance of the RFOB, the latter providing an estimate of the contact force, to be used in replacement of the actual measurement provided by a force sensor. The MEMS accelerometer is inexpensive and very compact.

Many researchers have proposed the use of acceleration measurement in a RFOB [(8)–(10)]. In particular, R. Oboe and D. Pilastro proposed a RFOB with acceleration-aided Kalman filter (aaKF) [(10)]. The aaKF can accurately estimate the position, velocity, and acceleration, even in presence of bias in measured acceleration. In their proposed solution, a disturbance observer (DOB) and a RFOB [(7)] are used in the control, with the RFOB in charge of the estimates of the reaction forces, arising from the contact with the environment.

We published the force control part for probing systems

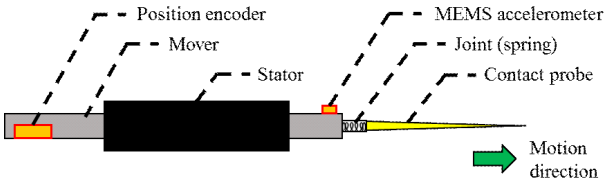

Fig. 1. Probing system

using combination of the aaKF and the RFOB in Ref. (11) and Ref. (12). This paper will elaborately describe the detailed analysis of the control technique. The proposed controller can be categorized in the following 5 stages.

Stage 1: PD position control before the contact
Stage 2: Impact detection
Stage 3: Negative force application
Stage 4: Hold mode
Stage 5: Force control based on aaKF and RFOB

The difference from Ref. (11) and Ref. (12) is as shown below:

- The mass of the mover of the linear motor was reduced by hardware modification.
- The friction force was reduced by hardware modification.
- The resonance frequency of the MEMS accelerometer becomes very high.

These improvements affected the control performance and better experimental data were obtained.

Experiments were conducted to validate the new proposed system and strategy, proving its effectiveness in achieving fast and precise force settling at the probe tip. Additional discussions are described in this paper.

This paper is organized as follows: Section 2 describes the modeling of the probing system for in-circuit testing. Section 3 explains the proposed fast force control in 5 stages. Experimental results are shown in Sect. 4. Discussions are reported in Sect. 5, and Sect. 6 concludes this paper.

2. Modeling of Probing System

This section describes the dynamic model of the probing system. Figure 1 shows the probing system in this study, which consists of a linear motor, a contact probe, a position encoder, and a linear MEMS accelerometer. It is worth noticing that the probe tip is connected to the mover of the linear actuator through a spring. The motion equations of the mover and the probe are as follows:

$$M_{\mathrm{m}}\ddot{x}_{\mathrm{m}} = K_{\mathrm{t}}I - F^{\mathrm{spr}} \cdots (1)$$

$$M_{\mathrm{p}}\ddot{x}_{\mathrm{p}} = F^{\mathrm{spr}} - F^{\mathrm{env}} \cdots (2)$$

where M and x denote mass and position. The subscript "m" and "p" mean the mover and the probe. K_{t} and I denote the thrust constant of the linear motor and the driving current, respectively. F^{env} is the force arising from the contact with the environment. F^{spr} denotes the elastic force generated by the joint spring, which is calculated as

$$F^{\mathrm{spr}} = K_{\mathrm{spr}}\left(x_0 - \left(x_{\mathrm{p}} - x_{\mathrm{m}}\right)\right) \cdots (3)$$

where K_{spr} and x_0 denote the elastic coefficient and the rest length of the spring, respectively. As shown in Eq. (1) and Eq. (2), this probing system is one of two-mass systems [13][14].

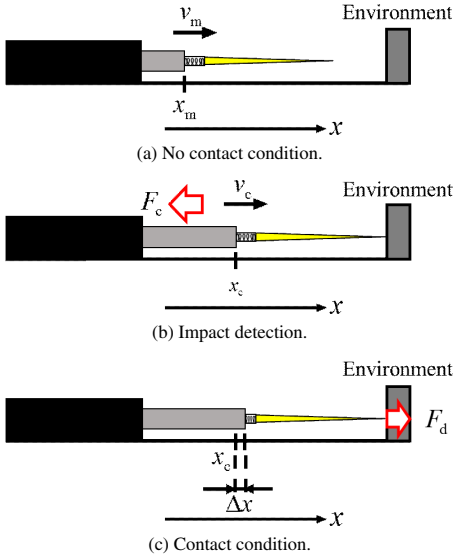

Fig. 2. Three conditions in probing operation

3. Fast Force Control

As mentioned in the introduction, we developed a new control strategy for probing systems in order to control the contact force instantaneously. Figure 3 shows the block diagram of the control system. $\hat{x}^{\mathrm{cmd}}$ and $\hat{F}_{\mathrm{d}}$ denote position command on no contact condition and desired contact force, respectively. s denotes Laplace operator. The symbols with "^" refer to the estimated values. The superscript "ref" means reference. The subscript "n" means nominal value. A DOB is used to achieve robust motion control [7], while the RFOB is used to estimate the environmental force. $\hat{F}^{\mathrm{dis}}$ and $\hat{F}^{\mathrm{env}}$ are disturbance force estimated by the DOB and environmental force estimated by the RFOB. The details of the DOB and the RFOB are described in Appendix 1. The fast force controller block calculates the acceleration reference $\ddot{x}^{\mathrm{ref}}$.

3.1 Calculation in Fast Force Controller

This subsection describes the calculation in the fast force controller. The contact operation can be divided into three conditions as shown in Fig. 2: no contact condition, impact detection, and contact condition. The acceleration reference $\ddot{x}^{\mathrm{ref}}$ is changed on each condition. The proposed control is categorized in 5 stages which are shown in the introduction.

Stage 1: Before the probe makes contact with the environment, a PD position control is applied. The acceleration reference is calculated as

$$\ddot{x}^{\mathrm{ref}} = K_{\mathrm{p}}\left(x^{\mathrm{cmd}} - \hat{x}_{\mathrm{m}}\right) + K_{\mathrm{v}}\left(\dot{x}^{\mathrm{cmd}} - \hat{\dot{x}}_{\mathrm{m}}\right) \quad \text{when } t < t_{\mathrm{c}} \cdots (4)$$

where K_{p} and K_{v} are PD control gains. $\dot{x}^{\mathrm{cmd}}$ and t_{c} denote the velocity command and the impact detection time.

Stage 2: The impact detection is conducted using the signals estimated by the aaKF. Before the contact, the probe is controlled in a forward direction, therefore the velocity is a positive value.

$$\hat{\dot{x}}_{\mathrm{m}} > 0. \cdots (5)$$

When the probe makes contact with the environment, impact force occurs. Due to this impact force, the acceleration

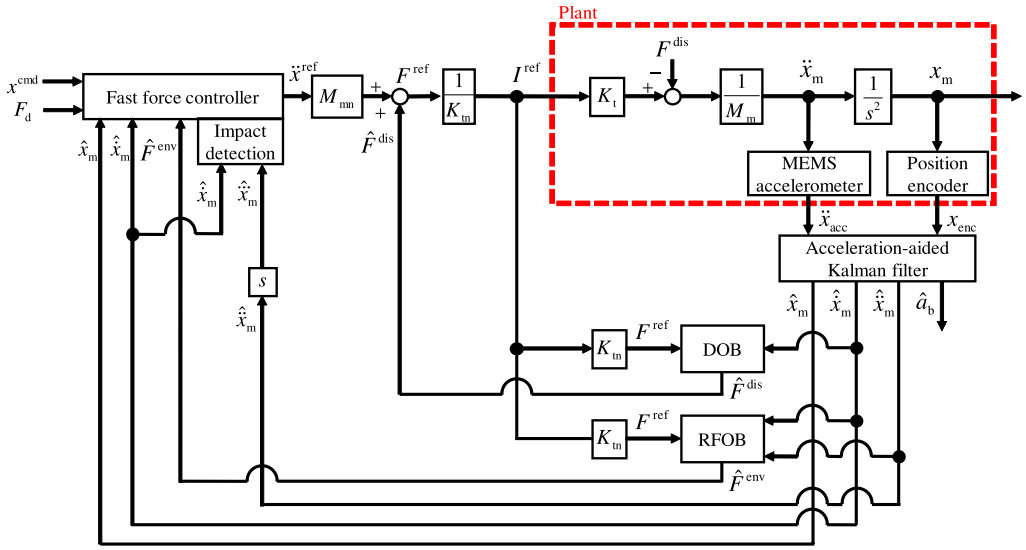

Fig. 3. Block diagram of control system

rapidly changes. Hence, the jerk signal which can be derived by differentiating the acceleration become large in a short period. The constraint of the jerk signal $\dddot{\hat{x}}_m$ can be expressed as

$$\left|\dddot{\hat{x}}_m\right| > \dot{a}_{th} \cdots\cdots (6)$$

where $\dot{a}_{th}$ is threshold value which is experimentally determined. The aaKF can reduce the measurement noise. Therefore, the jerk derived by differentiating the acceleration estimated by the aaKF has less noise than the jerk derived by differentiating the measured acceleration. The impact is detected using Eq. (5) and Eq. (6).

The RFOB can estimate the contact force. However, a LPF is usually applied to reduce the effect of the measurement noise. This LPF cut off the impact force, therefore the RFOB cannot detect the impact definitely.

Stage 3: After the contact detection, a negative constant force is applied in a short time to decelerate the mover. The value of the negative constant force is decided in terms of energy consumption. When the probe makes contact with the environment, the probe moves at a velocity v_c as shown in Fig. 2(b). The kinetic energy E_k can be calculated as

$$E_k = \frac{1}{2} M_m {v_c}^2 . \cdots\cdots (7)$$

In this paper, the mass of the contact probe M_p is much smaller than the mass of the mover, therefore, the kinetic energy of the probe is ignored. After the impact detection, the negative constant force $-F_c$ decelerates the mover motion. The energy loss by $-F_c$ is calculated as

$$E_l = -F_c \Delta x \cdots\cdots (8)$$

where Δx denotes the displacement from the contact detected position to the stop position. From Eq. (7) and Eq. (8), Eq. (9) can be derived.

$$E_k + E_l = \frac{1}{2} M_m {v_c}^2 - F_c \Delta x = 0. \cdots\cdots (9)$$

The velocity becomes zero after the negative force is applied. Therefore Eq. (10) can be obtained.

$$v_c + a t_s = 0 \cdots\cdots (10)$$

where a denotes deceleration caused by $-F_c$ which is calculated as

$$a = -\frac{F_c}{M_m} . \cdots\cdots (11)$$

t_s is the time when the mover stops. Solving Eq. (9) and Eq. (10) into F_c and t_s yields

$$F_c = \frac{M_m v_c^2}{2\Delta x} \cdots\cdots (12)$$

$$t_s = \frac{2\Delta x}{v_c} . \cdots\cdots (13)$$

When the mover stops, the probe pushes the environment with a desired force F_d to keep the contact. The pushing force is applied by the elastic force of the joint spring, therefore Δx is calculated as

$$\Delta x = \frac{F_d}{K_{spr}} . \cdots\cdots (14)$$

From Eq. (12) and Eq. (14), the acceleration reference in the deceleration mode can be calculated as

$$\ddot{x}^{ref} = -\frac{K_{spr} v_c^2}{2F_d} \quad \text{when } t_c \le t < t_c + t_s . \cdots\cdots (15)$$

Stage 4: After t_s from the impact detection, the hold mode is applied. Before the force control, this mode is required since the force estimated by the RFOB is not accurate when the acceleration reference is rapidly changed because of its LPF. In the hold mode, the velocity is controlled at 0 m/s for a short time t_h to keep the state. The acceleration reference of the hold mode is calculated as

$$\ddot{x}^{ref} = K_v \left(0 - \dot{\hat{x}}_m\right) \quad \text{when } t_c + t_s \le t < t_c + t_s + t_h . \cdots\cdots (16)$$

Stage 5: After the hold mode, the force control based on the aaKF and the RFOB is applied. The acceleration reference of the force control mode is calculated as

Table 1. Four controllers in experiments

	$t < t_c$	$t_c < t < t_c + t_s$	$t_c + t_s < t < t_c + t_s + t_h$	$t > t_c + t_s + t_h$
Conventional force control	Position control in Eq. (4)	Force control in Eq. (18)		
Conventional position control	Position control in Eq. (4)	Position control in Eq. (19)		
Proposed fast force control without hold mode	Position control in Eq. (4)	Deceleration mode in Eq. (15)	Force control in Eq. (17)	
Proposed fast force control with hold mode	Position control in Eq. (4)	Deceleration mode in Eq. (15)	Hold mode in Eq. (16)	Force control in Eq. (17)

$$\ddot{x}^{\mathrm{ref}} = K_{\mathrm{f}}\left(F_{\mathrm{d}} - \hat{F}^{\mathrm{env}}\right) \quad \text{when } t \geq t_{\mathrm{c}} + t_{\mathrm{s}} + t_{\mathrm{h}} \cdots\cdots\cdots\cdots\cdots\cdots (17)$$

where K_{f} denotes force control gain.

In ideal case, the contact force is controlled to the desired force at $t = t_{\mathrm{c}} + t_{\mathrm{s}}$. If there is a disturbance force such as modeling error and friction force, the force control compensates the disturbance force. Finally, it can be estimated that the force control will be completed in at least $t_{\mathrm{c}} + t_{\mathrm{s}} + t_{\mathrm{h}} + t_{\mathrm{RFOB}}$, where t_{RFOB} is the inverse of the LPF cutoff frequency of the RFOB.

4. Experiments

This section describes experimental results. The experiments were conducted to validate the proposed control strategy. Four controllers listed in Table 1 are compared; conventional force control, conventional position control, proposed fast force control without hold mode, and proposed fast force control with hold mode.

4.1 Experimental Setup This subsection explains the experimental setup. Figure 4 shows the experimental system, while Table 2 lists its components. It is worth noticing that a force sensor was used to measure the actual contact force. Therefore, it was not used for control purposes. The contact part of the force sensor is made of stainless steel. In the actual in-circuit tests, the probe tip contacts with a solder surface. The solder stiffness is different from the stainless stiffness, however, these stiffness is much larger than the stiffness of the spring. Hence, it is assumed that the stiffness difference does not affect the control performance.

Table 3 shows the parameters used in the experiments. Some of them (e.g. the control gains and the cutoff frequencies) were experimentally tuned. Additionally, the MEMS accelerometer was selected based on its resonant frequency of 22 kHz, which is higher than the Nyquist frequency of 5 kHz, to prevent aliasing issues.

The threshold value of the jerk signal $\dot{a}_{\mathrm{th}}$ was also experimentally decided. Firstly, $\dot{a}_{\mathrm{th}}$ was set at the maximum value of $\dddot{\hat{x}}_{\mathrm{m}}$ when the mover stops. Next, $\dot{a}_{\mathrm{th}}$ was set at the maximum value of $\dddot{\hat{x}}_{\mathrm{m}}$ in Stage 1.

In each controller, the impact detection was conducted using the constraints in Eq. (5) and Eq. (6). Additionally, position control is used on no contact condition. The position command was decided on the basis of the velocity command. At the beginning of the operation, the velocity command increases in proportion to the time. When the command becomes the target velocity, the velocity command is held constant. In this paper, the target velocity is set at 0.1 m/s.

4.2 Experimental Results Firstly, the results of a conventional force control are described. After the impact detection, the conventional force control was applied, whose acceleration reference is calculated as

$$\ddot{x}^{\mathrm{ref}} = K_{\mathrm{f}}\left(F_{\mathrm{d}} - \hat{F}^{\mathrm{env}}\right) \quad \text{when } t > t_{\mathrm{c}} \cdots\cdots\cdots\cdots\cdots (18)$$

Figure 5 shows the experimental results of the conventional force control. The thin line, thick line, and dot line in Fig. 5(a) denote the force estimated by the RFOB, the force measured by the force sensor, and desired force F_{d}. The thin

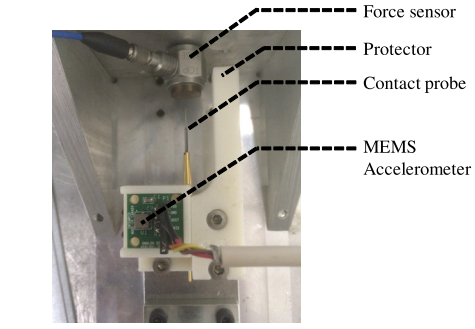

(a) Contact probe.

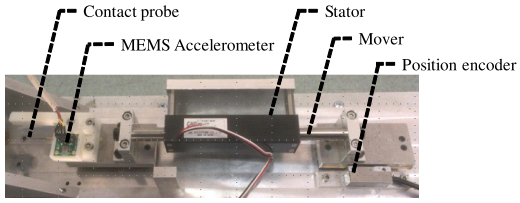

(b) General view.

Fig. 4. Experimental system

Table 2. Experimental equipments

Control board	PCI-6289 (National Instruments Co.)
Software	MATLAB/Simulink (The Mathworks, Inc.)
Contact probe	SPB B111 (SPEA)
Position encoder	RGH24X15A30D00A (Renishaw plc.)
MEMS accelerometer	ADXL001 (Analog Devices, Inc.)
Force sensor	208C01 (PCM Piezotronics, Inc.)

Table 3. Parameters

Sampling time	T_{s}	0.1 ms
Mass of the mover	M_{mn}	0.457 kg
Elastic coefficient	K_{spr}	500 N/m
Position control gain	K_{p}	400
Velocity control gain	K_{v}	40
Force control gain	K_{f}	1.0
Cutoff frequency of DOB	g_{DOB}	500 rad/s
Cutoff frequency of RFOB	g_{RFOB}	500 rad/s
Desired force	F_{d}	0.5 N
Hold time	t_{h}	15 ms
Threshold value of jerk signal	$\dot{a}_{\mathrm{th}}$	1.5×10^{4} m/s^3
A/D converter resolution		18 bits
Position encoder resolution	q	1 μm
Noise variance of position encoder	$q^2/12$	8.33×10^{-14} m^2
Noise variance of accelerometer		3.8857 m^2/s^4

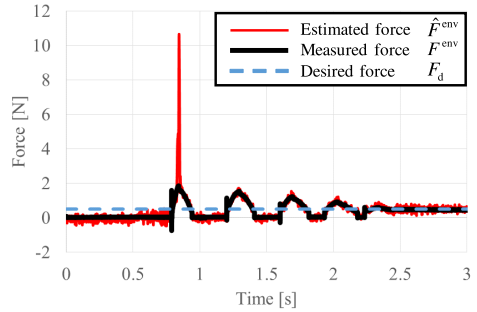

(a) Force response.

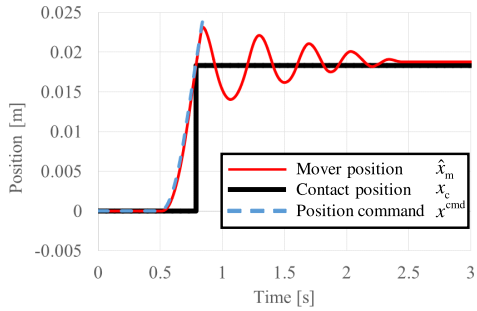

(b) Position response.

Fig. 5. Experimental results of conventional force control

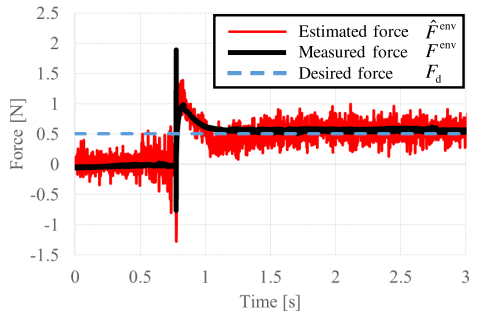

(a) Force response.

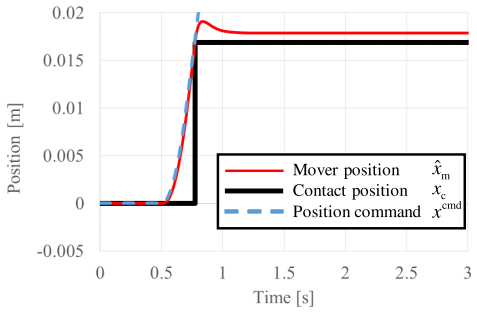

(b) Position response.

Fig. 6. Experimental results of conventional position control

line, thick line, and dot line in Fig. 5(b) denote the mover position, the detected position x_d, and position command on no contact condition. As the results, the force and position oscillate after the probe makes contact with environment. After 1.6 s from the impact detection, the force is controlled at the desired force. The overshoot of the measured force is 1.36 N. The estimated force became very large values at $t = 0.8$ s, this due to the fact that the mechanical limiter got in contact with the wall. Clearly, the overshoot and settling time should be smaller.

Next, the results using a conventional position control are described. After the impact detection, the conventional position control was applied, whose acceleration reference is calculated as

$$\ddot{x}^{ref} = K_p\left(x_d + \Delta x - \hat{x}_m\right) + K_v\left(0 - \hat{\dot{x}}_m\right) \quad \text{when } t > t_c. \cdots\cdots\cdots\cdots (19)$$

Figure 6 shows the experimental results of the conventional position control. The meaning of the lines in Fig. 6(a) and Fig. 6(b) is the same in Fig. 5(a) and Fig. 5(b). The settling time is 0.32 s which is shorter than the results of the conventional force control. The overshoot of the measured force is about 0.48 N. If used, this control strategy would damage the soldering point, therefore the overshoot should be smaller. In addition, there is 0.1 N error in steady state. It is worth noticing that the error comes from the detection delay. Additionally, a better accuracy of the force control is desirable.

Next, the results using proposed control without the hold mode are described. This experiment was conducted to confirm the effectiveness of the hold mode in Stage 3. Figure 7 shows the experimental results. The meaning of the lines in Fig. 7(a) and Fig. 7(b) is the same in Fig. 5(a) and Fig. 5(b). The responses are similar to the results of the conventional force control in Fig. 5. Figure 8 shows the enlarged view of Fig. 7(a) around the impact detection. At 0.798 s ($t = t_c + t_s$),

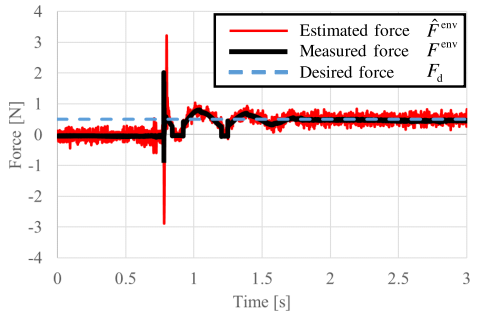

(a) Force response.

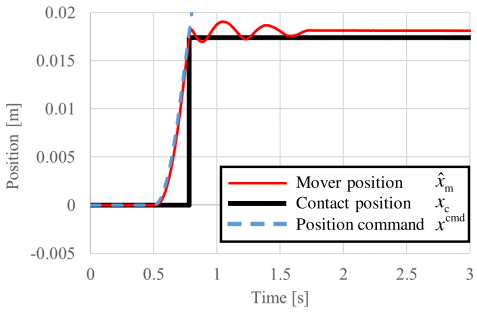

(b) Position response.

Fig. 7. Experimental results of proposed fast force control without hold mode

the control mode was switched from deceleration mode to force control mode. However, the estimated force by the RFOB became larger than the desired force, since the acceleration reference rapidly changed. Therefore, the acceleration reference calculated by Eq. (17) becomes a negative value, and the probe did not keep the contact.

Finally, the results of the proposed control with hold mode are described. Figure 9 shows the experimental results. The meaning of the lines in Fig. 9(a) and Fig. 9(b) is the same in Fig. 5(a) and Fig. 5(b). From Fig. 9(a), the settling time and

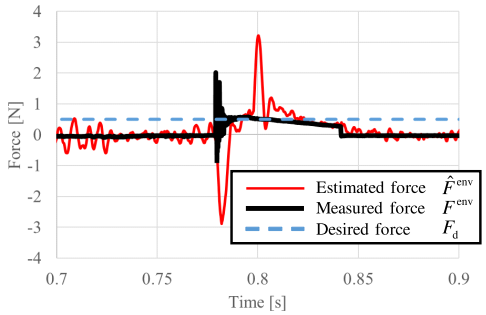

Fig. 8. Enlarged view of Fig. 7(a)

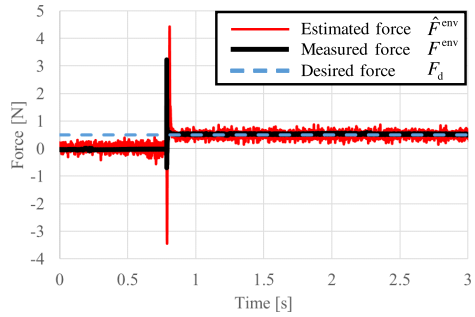

(a) Force response.

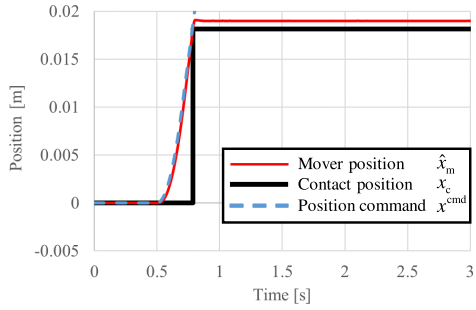

(b) Position response.

Fig. 9. Experimental results of proposed fast force control with hold mode

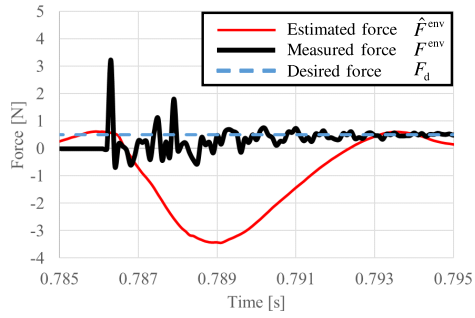

Fig. 10. Enlarged view of Fig. 9(a)

overshoot is very small. Fig. 10 is the enlarged force response shown in Fig. 9(a). The settling time of the measured force is about 10 ms. In addition, there is no overshoot in the measured force. Therefore, the proposed fast force control can quickly control the force with no overshoot.

In the transient state, the estimated force become very large. The reason is that the acceleration reference is rapidly changed at $-F_c$ as shown in Eq. (15). However, the DOB and RFOB have a LPF, whose cutoff frequencies are 500 rad/s. Therefore, the rapid change cannot be observed. The calculated value of t_d and the hold time t_h are 18.5 ms and 15 ms,

Table 4. Summary of experimental results

	Overshoot	Settling time
Conventional force control	more than 1.36 N	1.6 s
Conventional position control	0.48 N	0.32 s
Proposed force control	no overshoot	within 10 ms

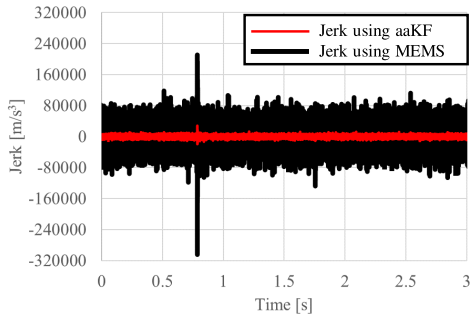

Fig. 11. Comparison of jerk signal

respectively. Hence, the estimated value in 33.5 ms after the impact detection is not used in the control. The estimated force at the time of the mode change is the same value of F_d. Therefore, the mode change was smoothly implemented.

5. Discussions

This section describes the discussions of the experimental results.

5.1 Overshoot and Settling Time Table 4 shows the comparison of the overshoot and the settling time of the measured force in each experimental result. It is clearly shown that the proposed controller is superior to the other controllers from viewpoints of the overshoot and the settling time.

5.2 Delay of Impact Detection in Stage 2 In the proposed method, the impact detection was conducted using Eq. (5) and Eq. (6). This subsection discusses about the delay of the impact detection.

Firstly, Fig. 11 shows the comparison of the jerk signals calculated by using the measured acceleration and the aaKF estimated acceleration when the proposed controller was implemented. The thin line and the thick line denote the jerk calculated by using the measured acceleration and the jerk calculated by using the aaKF estimated acceleration, respectively. It can be confirmed that the jerk signal calculated by using the estimated acceleration is much clear than one calculated by using the measured acceleration. The standard deviation of the jerk signals calculated by using the measured acceleration and the estimated acceleration before the operation ($0 < t < 0.5$) are 2.741×10^4 m/s^3 and 2.728×10^3 m/s^3, respectively. Hence, it is clear that the aaKF can reduce the noise. Additionally, the aaKF can compensate the bias of the acceleration, therefore, the threshold value for the impact detection can be set at a constant value.

Around 0.8 s, the jerk signal rapidly changed because of the impact force. The time of the impact detection by Eq. (5) and Eq. (6) is 0.7864 s. On the other hand, the actual impact detection time can be measured using the force sensor. When the impact force occurs, the measured force is largely changed as shown in Fig. 10. The actual impact detection time is 0.7863 s. Therefore, the time difference is only one sampling time of 0.1 ms. In other words, the impact detection by using the aaKF estimation signals is almost equivalent

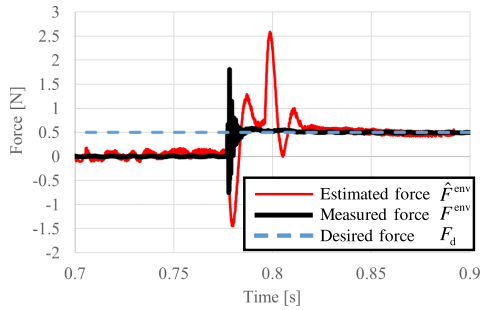

(a) Response when standard RFOB is used.

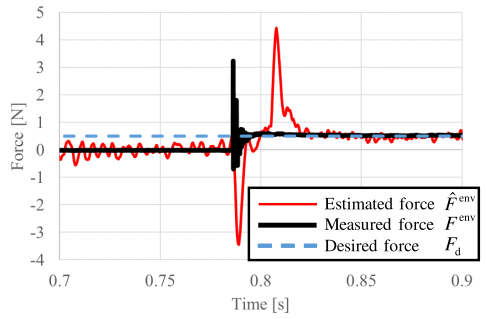

(b) Response when aaKF RFOB is used.

Fig. 12. Comparison of force response around impact detection

with the impact detection by using the force sensor.

5.3 Comparison of Standard RFOB and aaKF RFOB

This subsection describes the comparison of standard RFOB (SRFOB) and aaKF RFOB. Figure 12 shows the comparison of the force response of the fast force control using the SRFOB and the aaKF RFOB around the impact detection. As a result, both the SRFOB and the aaKF RFOB could estimate the contact force in steady state, and the contact force was controlled. However, the force estimated by the SRFOB is oscillatory because of the pseudo differentiation, which is used to calculate the velocity from the position information. Additionally, the settling time of the estimated force by the SRFOB is longer than one by the aaKF RFOB. Therefore, the hold time t_h should be set longer. Hence, the aaKF RFOB is suitable for the proposed fast force control.

6. Conclusions

This paper proposed a fast force control without force sensor for probing system. In order to estimate the contact force, a RFOB is utilized. A MEMS accelerometer is used to improve the performance of the RFOB. Additionally, the aaKF is used to estimate the position, velocity, and acceleration accurately. A conventional force control, a position control, and the proposed fast force control were compared by the experiments. As the results, the proposed controller achieved the fastest force control compared with the other controllers, with 10 ms settling time and no overshoot. Therefore, the proposed control does not damage the contacted environment. It was also confirmed that the impact detection using the aaKF signals was achieved with only one sample delay.

This proposal is useful for the in-circuit test with the probing systems since the contact force can be controlled with very short settling time and without overshoot.

References

(1) J.E.M. Martin, A.S. Nevado, and A.V. Martinez: "Low cost programmable modular system to perform In-Circuit Test (ICT) full development of the hardware, software and mechanics of an ICT machine", In Proc. of Technologies Applied to Electronics Teaching, TAEE2016, pp.1–7 (2016)

(2) Q. Yuan, L. Han, J. Li, and D. Ge: "Real-time voltage and resistance features in microprobe testing process", *IEEE Trans. Components, Packaging and Manufacturing Technology*, Vol.5, No.2, pp.274–278 (2015)

(3) Y. Hiratsuka, F. Katoh, K. Konishi, and S. Shin: "A design method for minimum cost path of flying probe in-circuit testers", In Proc. of SICE Annual Conference 2010, pp.2933–2936 (2010)

(4) J.H. Shim, H.S. Cho, and S. Kim: "An actively compliable probing system", *IEEE Control Systems*, Vol.17, No.1, pp.14–21 (1997)

(5) N. Shimada, T. Yoshioka, K. Ohishi, and T. Miyazaki: "Novel force-sensorless contact motion control for quick and smooth industrial robot motion", In Proc. of the 37th Annual Conference on IEEE Industrial Electronics Society, IECON2011, pp.4238–4243 (2011)

(6) G.A. Gardona, W. Moreno, A. Weitzenfeld, and J.M. Calderon: "Reduction of impact force in falling robots using variable stiffness", In Proc. of SouthEastCon 2016, pp.1–6 (2016)

(7) S. Katsura, Y. Matsumoto, and K. Ohnishi: "Modeling of force sensing and validation of disturbance observer for force control", *IEEE Trans. Ind. Electron.*, Vol.54, No.1, pp.530–538 (2007)

(8) T.T. Phuong, C. Mitsantisuk, and K. Ohishi: "High performance force sensing based on Kalman-filter-based disturbance observer utilizing FPGA", *IEEJ Transactions on Industry Applications*, Vol.131, No.3, pp.334–342 (2011)

(9) D. Pilastro R. Oboe, R. Antonello, and K. Ito: "Use of MEMS inertial sensors for performance improvement of low-cost motion control systems", *IEEJ Journal of Industry Applications*, Vol.5, No.2, pp.78–89 (2016)

(10) R. Oboe and D. Pilastro: "Performance improvement of haptic device in bilateral control using aaKF and RFOB", In Proc. of the 42nd Annual Conference of IEEE Industrial Electronics Society, IECON2016, pp.0–7 (2016)

(11) S. Nagai, R. Oboe, T. Shimono, and A. Kawamura: "Force sensorless fast force control for probing systems using aaKF", In Proc. of IEEJ International Workshop on Sensing, Actuation, Motion Control, and Optimization, SAMCON2017, No. TT3-6, pp.1–6 (2017)

(12) S. Nagai, R. Oboe, T. Shimono, and A. Kawamura: "Fast force control using acceleration-aided Kalman filter and reaction force observer for probing systems", In Proc. of the 43rd Annual Conference of IEEE Industrial Electronics Society, IECON2017, pp.4037–4042 (2017)

(13) S. Katsura and K. Ohnishi: "Force control by flexible manipulator based on resonance ratio control using position sensitive detector", *IEEJ Transactions on Industry Applications*, Vol.126, No.6, pp.693–699 (2006)

(14) S. Yamada and H. Fujimoto: "Design of load-side external force observer with a load-side encoder considering modeling errors", In Proc. of the 43th Annual Conference on IEEE Industrial Electronics Society, IECON2017, pp.7589–7595 (2017)

Appendix

1. DOB and RFOB

In this section, some simplifications of the model described in Sect. 2 is described, in order to achieve a simpler implementation of the DOB and RFOB that is used in the proposed control. In this paper, the mass of the contact probe is much smaller than the mass of the mover, therefore the inertial force of the probe $M_p\ddot{x}_p$ can be neglected. The motion equations Eq. (1) and Eq. (2) can be rewritten as

$$M_m\ddot{x}_m = K_t I - F^{env} \cdots\cdots (A1)$$

$$F^{spr} = F^{env}. \cdots\cdots (A2)$$

Eq. (A1) is the same as the motion equation of a linear motor. Hence, the DOB and the RFOB can be applied in the same way of Ref. (7).

app. Fig. 1 shows the block diagram of the SRFOB [7]. g_{RFOB} denotes the cutoff frequency of the RFOB. In order to calculate the velocity from the position information, a pseudo differentiation (whose cutoff frequency is g_{dif}) is often used. However, this causes an estimation delay. On the other hand,

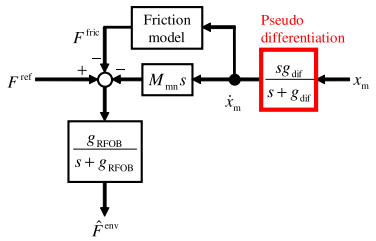

app. Fig. 1. Block diagram of standard RFOB (SRFOB)

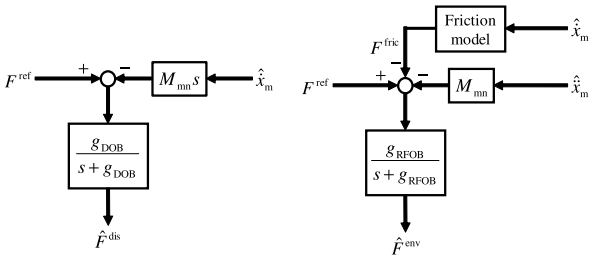

(a) DOB. (b) RFOB.

app. Fig. 2. Block diagram of DOB and RFOB used in proposed fast force control

the aaKF can directly estimate the velocity and the acceleration, therefore the pseudo differentiation is not required by combining the aaKF and the RFOB as shown in Fig. 2. As a result, the aaKF RFOB can estimate the reaction force more accurately.

app. Fig. 2 shows the block diagram of the DOB and RFOB used in the proposed control. $\hat{F}^{\mathrm{dis}}$ denotes the estimated disturbance force, such as nominal error, friction, and reaction force from the environment. g_{DOB} denotes the cutoff frequency of the DOB. The friction force F^{fric} includes the coulomb friction and the viscous friction, which is calculated as

$$F^{\mathrm{fric}} = f_{\mathrm{c}}\mathrm{sign}\left(\dot{x}_{\mathrm{m}}\right) + D\dot{x}_{\mathrm{m}} \cdots\cdots\cdots\cdots\cdots\cdots\cdots\cdots \text{(A3)}$$

where f_{c} and D denote the coefficient of the coulomb friction and the viscous friction.

Sakahisa Nagai (Student Member) received the B.E. degree in faculty of engineering in 2014 and the M.E. degree in graduate school of engineering in 2016 from Yokohama National University, Kanagawa Japan. He is now a Ph.D. course student in the same university. He has belonged to the Kawamura laboratory since April 2013. His research interests include sensorless actuation and motion control.

Roberto Oboe (Member) was born in Lonigo, Italy, on October 26, 1963. He received the Laurea degree (cum laude) in Electrical Engineering and the Ph.D. degree from the University of Padova, Padova, Italy, in 1988 and 1992, respectively. He is presently Associate Professor of Automatic Control at the Department of Management and Engineering of the University of Padova, Vicenza, Italy. His research interests are in the fields of motion control, telerobotics, haptic devices, rehabilitation robots and applications and control of MEMS.

Tomoyuki Shimono (Senior Member) received the B.E. degree in mechanical engineering from Waseda University, Tokyo, Japan, in 2004 and the M.E. and Ph.D. degrees in integrated design engineering from Keio University, Yokohama, Japan, in 2006 and 2007, respectively. From 2007 to 2008, he was a Research Fellow of the Japan Society for the Promotion of Science. From 2007 to 2008, he was also a Postdoctoral Fellow at Keio University. From 2008 to 2009, he was a Research Associate with the Global Centers of Excellence Program, Keio University. Since 2009, he has been with the Department of Electrical and Computer Engineering, Yokohama National University, Yokohama, where he is currently an Associate Professor. He has also been a project leader of Kanagawa Institute of Industrial Science and Technology since 2016. His research interests include haptics, motion control, medical and rehabilitation robots, and actuators.

Atsuo Kawamura (Fellow) received the Ph.D. degree in electrical engineering from the University of Tokyo in 1981. After the five-year-stay at the University of Missouri-Columbia as a faculty member, he joined Yokohama National University in 1986, and in 1996 he became a professor. From 2013 to 2015 he was a dean of College of Engineering Science and also a dean of Graduate School of Engineering at Yokohama National University. He has also been a project member of Kanagawa Institute of Industrial Science and Technology since 2016. His interests are in the fields of power electronics, digital control, electric vehicles, and biped robotics. He received Transactions Paper Awards from IEEE in 1988, 2001 and 2002, also from IEE of Japan in 1996. Dr. Kawamura is an IEEE Fellow, and also a Fellow of the IEE of Japan. He served as a president of IEEJ/IAS from May 2012 to May 2013.